remote sensing

MDPI

Article

Seasonality and Characterization Mapping of Restored Tidal Marsh by NDVI Imageries Coupling UAVs and Multispectral Camera

William Nardin [1,*], Yuri Taddia [1,2], Michela Quitadamo [1,2], Iacopo Vona [1], Corinne Corbau [1,3], Giulia Franchi [4], Lorie W. Staver [1] and Alberto Pellegrinelli [2]

1 Horn Point Laboratory, Center for Environmental Science, University of Maryland, Cambridge, MD 21613, USA; yuri.taddia@unife.it (Y.T.); mquitadamo@umces.edu (M.Q.); ivona@umces.edu (I.V.); cbc@unife.it (C.C.); lstaver@umces.edu (L.W.S.)
2 Engineering Department, University of Ferrara, 44122 Ferrara, Italy; alberto.pellegrinelli@unife.it
3 Department of Physics and Earth Sciences, University of Ferrara, 44122 Ferrara, Italy
4 Department of Computer Science, Salisbury University, Salisbury, MD 2180, USA; gxfranchi@salisbury.edu
* Correspondence: wnardin@umces.edu

Abstract: Salt marsh evolution is strongly affected by tidal processes and ecology, which regulate sediment accretion and erosional rates. A balance between marsh erosion and deposition in a restored tidal wetland is crucial for analyzing restoration strategies to adopt in a natural context. Here, we present an integrated approach monitoring salt marsh seasonal changes over several months in a microtidal restored salt marsh of the Paul S. Sarbanes Ecosystem Restoration Project at Poplar Island (MD, USA). The project is undertaken at a restoration site where sediment dredged from the shipping channels in the upper Chesapeake Bay is being used to restore a tidal marsh habitat in mid-Chesapeake Bay. We flew an Unmanned Aerial Vehicle (UAV) with an RGB and a multispectral camera to obtain a high-resolution map of the planimetric position of vegetation and to monitor the health of the marsh vegetation in diverse seasons. Due to its extension of 400 m by 400 m, a total of four flight plans were necessary to cover the entire marsh flying at a 40 m altitude obtaining a 2 cm Ground Sample Distance (GSD). This technique provides reliable results at a very low cost, enabling an accurate assessment of the marsh platforms to be conducted over time, due to both the very high spatial resolution and the precise georeferencing of the images for the comparisons. Our results show seasonal variability in the two dominant species colonizing the low marsh, *Spartina alterniflora*, and high marsh, *Sporobolus pumilus*. While the lower marshes showed a higher variability along seasons, the up-land vegetation showed persistent green foliage during cold seasons. Detecting salt marsh evolution and seasonality coupled with field measurements can help to improve the accuracy of hydrodynamic and sediment transport models. Understanding the drivers of salt marsh evolution is vital for informing restoration practices and designs, in order to improve coastal resilience, and develop and coastal management strategies.

Keywords: salt marsh restoration; vegetation monitoring; NDVI; Unmanned Aerial Vehicle (UAV); aerial photogrammetry; coastal morphodynamics; ecogeomorphology

Citation: Nardin, W.; Taddia, Y.; Quitadamo, M.; Vona, I.; Corbau, C.; Franchi, G.; Staver, L.W.; Pellegrinelli, A. Seasonality and Characterization Mapping of Restored Tidal Marsh by NDVI Imageries Coupling UAVs and Multispectral Camera. *Remote Sens.* **2021**, *13*, 4207. https://doi.org/10.3390/rs13214207

Academic Editors: Justin F. Moat and Alfredo Huete

Received: 3 August 2021
Accepted: 14 October 2021
Published: 20 October 2021

1. Introduction

Coastal regions are affected by a multitude of phenomena that significantly modify the dynamics of sediment transportation, such as storm surges, tidal processes and sea level rise [1–4]. Tidal wetland ecosystems, which are an integral part of many coastal systems, can also impact sediment dynamics, as well as promote biodiversity, enhance water quality, buffer coastal communities against sea level changes and storms, promote recreation and tourism and are recognized as an important blue carbon sink globally [5,6].

Chesapeake Bay, where extensive tidal wetlands are located, experiences sea level rise (SLR) at rates three to four times higher than the global average, presenting a challenge

to the resilience of coastal habitats [7]. The loss of hundreds of low-lying islands in the Chesapeake Bay (Maryland) are attributed to the action of inundation, wave erosion and historic SLR, and thousands more acres of coastal wetlands are projected to be eroded in the coming decades as SLR accelerates [8,9]. Some communities on Chesapeake Bay islands have been completely abandoned, while others have persevered by armoring island coastlines to limit shoreline erosion. In recent decades, creating and restoring tidal wetlands has been undertaken to replace important habitat associated with these lost islands, but understanding the complex dynamics in tidal wetlands will be important to insure resilience.

The combined effect of changing coastal hydrodynamics, sediment dynamics and ecological change (e.g., loss of submersed aquatic vegetation) within a coastal region could lead to increasing rates of erosion of the shoreline in certain areas. Therefore it is crucial to better understand the drivers of this process and to adopt efficient countermeasures for the successful restoration of the natural protection offered by well-vegetated systems along the coast [4,10]. Recent modeling efforts and field studies have been dedicated to better understanding the processes driving tidal marsh development [11].

Biological and geomorphic dynamics that lead to tidal wetland development under different local conditions have been explored [3,12–15]. These studies mostly reveal an inverse correlation between water fluxes and marsh density and examine the effects of marsh canopy on the turbulence [16]. Tidal vegetation slows water velocities, changes water fluxes and dissipates wave energy, especially along the marsh edges [2,4,17]. Plant morphology, such as leaf and stem dimensions, can also impact wave attenuation and sediment dynamics [18]. The interactions between vegetation and hydrodynamic processes are the main drivers of tidal system morphodynamics [15].

Quantitative models of marsh evolution are crucial to predict the fate of these vulnerable coastal systems. One of the key difficulties in our capability to estimate tidal marsh development is the lack of spatially relevant data showing the complexity of these important coastal systems. Aerial photogrammetry might potentially play an important role in future studies regarding tidal marsh evolution, enhancing the current level of information available.

Remote sensing images (Landsat, Sentinel2, MODIS), with resolutions of several meters, cannot detect small geomorphic features on the scale of a few centimeters. Yet, many previous studies have relied on passive remote sensing data from traditional satellites to map coastal salt marshes [19,20], or tropical zones characterized mainly by mangrove forest [21]. While traditional satellite data cannot provide the fine spatial resolution required to detect the complexity of marshes and wetlands, the development of Unmanned Aerial Vehicles (UAVs), combined with new sensors, in the last decade has revolutionized ecological and environmental monitoring [22]. UAVs can be used to survey limited areas frequently with high spatial resolution, which means this new tool has potential applications in diverse fields, including precision agriculture and ecological restoration [23].

Recently, monitoring of restored tidal marshes has been a focal point for many restoration projects around the US [3,24]. The combination of UAVs to acquire very high resolution aerial imagery of restoration sites combined with more traditional Global Navigation Satellite System (GNSS) geodetic receivers in Real Time Kinematic (RTK) mode to survey the position of vegetative species allows improved accuracy for mapping the marsh vegetation community [25,26].

Previous work in coastal management and habitat restoration have confirmed the effective application of UAVs as a tool for high resolution mapping. For instance, UAV imagery has been applied to monitor creek-marsh interactions and creek evolution in a tidal marsh [22], and to assess habitat diversity and ecosystem productivity [27]. Additionally, UAVs have been used successfully to detect multiple invasive species [28]. Other applications used multispectral cameras to map vegetation communities, and to quantify and monitor the production of biomass by coastal and upland vegetation [29,30]. These

studies mainly aim to predict plant spatial distribution, species change and biomass using the spectral characteristics of the vegetation.

The current use of in situ ground surveys, including standard plot-based marsh survey methods, in combination with UAV-based analyses is enhancing monitoring of forests and wetlands. The application of this new integrated approach for restored tidal marsh monitoring is expected to add new knowledge for wetland restoration and management [31,32]. Our study proposes a new methodology to include UAVs for detecting changes in vegetation distribution and characterization, and ecosystem functioning in a restored coastal marsh, opening a new window of opportunity for real-time coastal monitoring and management.

The ultimate goal of the work presented here is to assess seasonal change in a restored salt marsh. We applied in-situ field measurements of vegetation and marsh platform elevation to inform a remote sensing investigation into the factors that influence marsh evolution and impacts on sediment transport in a created marsh in mid-Chesapeake Bay (Figure 1). We monitored the two dominant plant species, *Spartina alterniflora* (syn. *Sporobolus alterniflorus*), in the low marsh and the high marsh species, *Sporobolus pumilus* (syn. *Spartina patens*), in different seasons.

A comparison with the initial as-built survey of the marsh in 2013 was used to detect changes from the original planting design, which had occurred by the date of our survey in 2019. The precision of the technique presented was sufficient to detect the magnitude of ecological and geomorphological changes in the study site during a year-long monitoring study. Our immediate objective was to identify the most appropriate time of year for obtaining imagery to differentiate the two *Spartina* species, with the broader goals of distinguishing high and low marsh zones, and tracking the geomorphological evolution of the marsh.

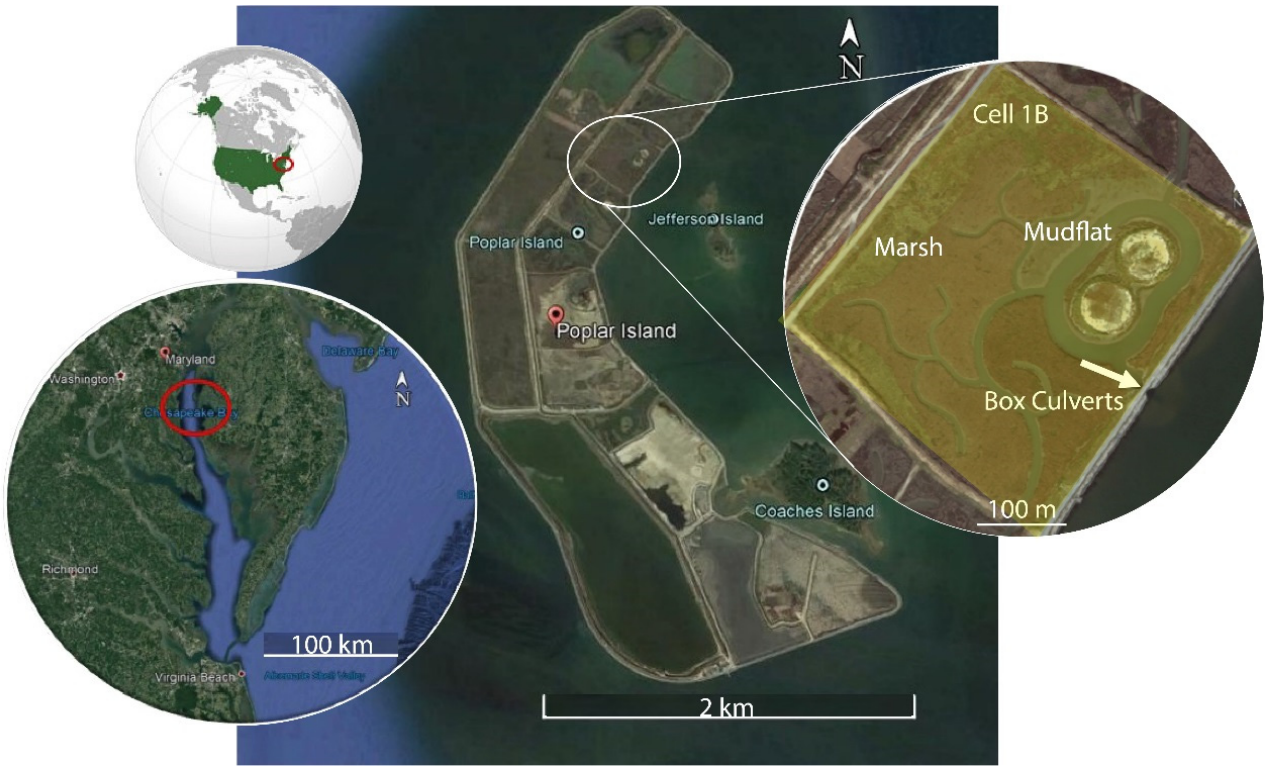

Figure 1. Poplar Island in the upper part of Chesapeake Bay (Maryland, US East Coast). The study site is on Poplar Island is the Cell 1B (highlighted in yellow color in the zoomed plot), in the northern part of the island (images courtesy of Google Earth and U.S. Army Corps of Engineers). Box culverts location shows the tidal inlet connecting the marsh with the Chesapeake Bay.

2. Materials and Methods

2.1. Study Site

The Paul S. Sarbanes Ecosystem Restoration Project at Poplar Island (Poplar Island) is an ecosystem restoration site constructed of sediment that is dredged from the navigation channels approaching Baltimore Harbor, intended to restore remote island habitat in the Chesapeake Bay. Currently spanning 5.6 km by 0.8 km, Poplar Island was once representative of numerous islands throughout the region (Figure 1) that have been subjected to severe erosion and inundation by rising sea levels. It is a beneficial use of dredged material project sponsored by the U.S. Army Corps of Engineers (USACE) and the Maryland Department of Transportation Maryland Port Administration (MDOT MPA) with the aim of restoring the earliest mapped extent of Poplar Island (1847). From the year 2000, the supply of dredged material resulting from the maintenance dredging of the shipping channels approaching Baltimore Harbor has enabled the recovery of a significant part of the initial island's surface (Figure 1).

The island is subdivided into diked units referred to as containment cells, which were created to confine the dredged material slurry during placement (Figure 1, Cell 1B highlighted in yellow color in the zoomed plot). When the project is complete, approximately half the area will be tidal marsh and half upland habitat. By 16 May 2017, 24.47 Million Cubic Meters (MCM) of fine-grained (median sand <10%, [33]) dredged materials have been placed on Poplar Island. When complete, approximately 694 ha of upland, wetland and embayment habitat will be restored [34]. Our measurements come from a single tidal marsh, Cell 1B, with neighboring marshes connected by two channels, one to the North (NE) and one to the South (SE), and two adjacent 1.8 m^2 box culverts that connect the marsh to the Chesapeake Bay (Figure 1). Cell 1B was graded and opened to tidal exchange in 2011 and planted with nursery grown *S. alterniflora* (low marsh) and *S. pumilus* (high marsh) in 2012.

The mean great diurnal tide range (difference between mean higher high water (MHHW) and mean lower low water (MLLW)) at this site is 0.468 m [35]. Target elevations were: high marsh 0.75 m above MLLW, low marsh 0.57 m above MLLW, with flooding typically occurring twice per day in the low marsh and once per day in the high marsh. Preliminary surveys and hydrodynamic modelling in, and around, Poplar Island have provided a useful, but incomplete picture of the environmental forces sculpting the marsh complex. At present, the ecology, the hydro-dynamics and the sediment transportation of the Poplar Island salt marshes are extensively investigated by scientists in support of an adaptive management program. The marshes have been developed sequentially and represent a unique environment where various restoration interventions have been utilized and are currently being assessed.

2.2. Field Survey

For comparison with imagery obtained by UAV, marsh vegetation in the two zones populated by *S. alterniflora* and *S. pumilus* was characterized on 10 dates from April 2019 to November 2019 in different seasons to capture temporal variation and tidal variability (Figure 2).

Vegetation sampling points were established in areas with the two main marsh species (Figures 3 and 4). Measurements of stem density, canopy height, and stem diameters were recorded at variable intervals using 0.01 m^2 quadrats (Figure 2b,c). Stem densities were determined by counting each stem inside the quadrat. Canopy height was determined by averaging the heights of the five tallest individual stems within each quadrat. Mean stem diameter was calculated from measurements taken on ten stems per quadrat at a height of 15 cm from the soil surface using a Vernier caliper. Measured vegetative characteristics were used to calculate vegetation volume, to validate UAV imagery.

Figure 2. (**A**) GNSS ground survey in RTK mode on November 2019; (**B**) measurement of stem height; (**C**) measurement of stem density with a quadrat.

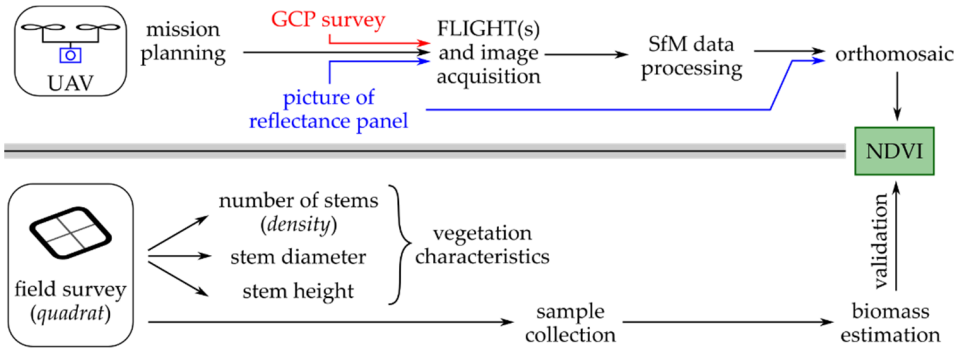

Figure 3. Flow chart of the field and photogrammetry analysis and validation.

To compare different runs with multiple vegetation species, we define a vegetation volume, Vv, as:

$$V_v = n\, h_v \tag{1}$$

where $n = m\, D$ is the vegetation density, h_v is the stem height, m is the number of stems per unit area, and D is the stem's diameter.

Marsh elevation and Ground Control Point (GCP) positions were measured within the marsh complex using a geodetic GNSS (GPS + GLONASS) receiver Topcon Hiper V in RTK mode. The RTK georeferenced tidal marsh points in NAVD88 datum, allowing

us to empirically determine vegetation sample stations (Figure 2a). The base station was placed on known coordinates (Poplar Island benchmark CM 2: https://www.ngs.noaa.gov/NGSDataExplorer/, accessed on 2 July 2021) located on the western side of Cell 1B (Figure 4). Within the tidal marsh area, we used a rover receiver mounted on an extendable pole to survey position and elevation (Figure 2a).

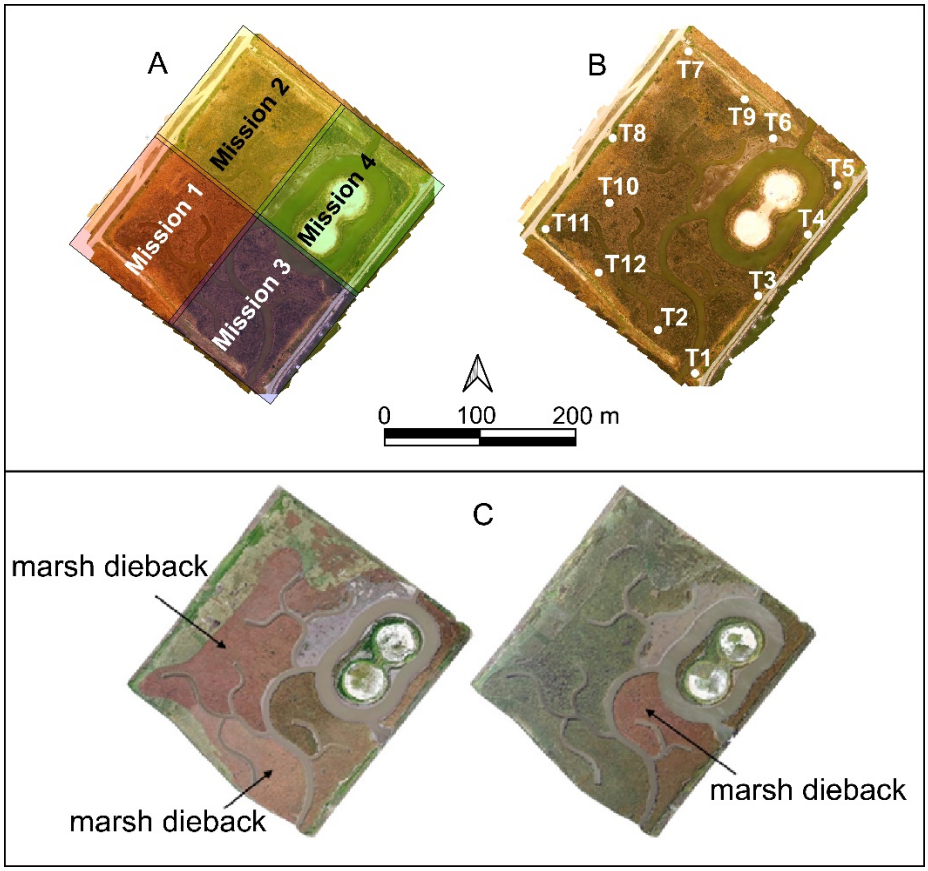

Figure 4. (**A**) Scheme of the planned flight missions (Pix4D Capture). (**B**) Position of GCPs for the UAV survey in November 2019. (**C**) Images of Cell 1B from September 2013 on the left and September 2014 on the right. Black arrows point to marsh areas affected by vegetation dieback, which are represented by brown senescent plants of *S. alterniflora*.

2.3. UAV Surveys and Data Analysis

A photogrammetric technique was adopted for the detection of the topography of Cell 1B in Figure 1 [36–39]. Due to the recent availability of lightweight and compact digital cameras and the continuous development of algorithms in the computer vision, a Structure from Motion (SfM) approach was followed [40–42].

The SfM process is an advanced method able to exploit a set of images. It enables a 3D geometry (the so-called structure) reconstruction from a set of 2D images of the scene (the so-called motion). The detection of the tie points by image-matching algorithms that look for features between multiple images, and recognition of the same feature at different image scales, represents the first step. The reconstruction of the geometry does not need any a-priori assumption, such as a set of GCPs (Figure 4) and the traditional collinearity equations can be solved in an arbitrary scale. SfM additionally estimates the interior orientation of the camera, as well as the exterior orientation of each imagery at the end of a bundle adjustment [43]. This implies that the method can be used for uncalibrated commercial cameras, since the SfM process will self-calibrate it (Figure 3).

The use of UAV acquired images is particularly beneficial when combined with SfM techniques and provides high spatial resolution at a low cost [44,45]. For the above reasons, a DJI Phantom 3 Professional (DJI-P3P) was used for the aerial survey of the site. Four

different flight missions (Figure 4) were necessary to complete the data acquisition due to the cell's extent of about 400 m by 400 m. A proper overlap between border strips of a flight plan with the previous and the following ones ensured the lack of any uncaptured area. The main parameters set for the flight plans were as follows: Longitudinal overlap 80%, side overlap 60% and flight altitude 40 m.

The DJI-P3P drone was also equipped with a MicaSense RedEdge-M multispectral camera. This camera allows one to collect information in the near infrared wavelengths (NIR), in particular the NIR band captured by the MicaSense RedEdge-M has a central value of 840 nm and a Full-Width Half-Maximum (FWHM) of 40 nm. The number of flight missions mentioned above took into account the presence of an additional camera payload that reduced the actual flight autonomy of the aircraft.

The Ground Sample Distance (GSD), that represents the pixel size on the ground, can be computed as:

$$GSD = ps * \frac{H}{c} \quad (2)$$

where ps = pixel size on the sensor array (m); H = flight altitude (m); and c = focal length of the camera (m). Due to the camera specifications reported in Table 1, the resulting GSD of both cameras is respectively of ≈1.8 cm for the DJIFC300 and ≈2.8 cm for the Micasense RedEdge-M. Pix4D Capture app was used for mission planning.

Table 1. Aircraft and camera specifications.

Aircraft Specifications		
Type		**DJI Phantom 3 Professional**
Take off weight		1280 g
Max flight speed		16 m/s
Max flight time *		18–20 min
Hovering accuracy	Horizontal	±0.3–1.5 m
	Vertical	±0.1–0.5 m
Camera Specification		
Name	**DJI FC300X**	**MicaSense RedEdge-M**
Type	**RGB**	**Multispectral with Global Shutter**
Focal length	3.6 mm	5.5 mm
35 mm equiv. focal length	20 mm	39.7 mm
Image resolution	4000 × 3000	1280 × 960
Field of view	84°	48.8°
GSD at 40 m altitude	≈1.8 cm	≈2.8 cm

* the actual flight time was reduced when using the MicaSense RedEdge-M.

The reconstruction of the photogrammetric model was performed using Agisoft PhotoScan/Metashape Professional. To georeference the model, GCPs were introduced. An additional set of check points (CPs) was also surveyed to assess the achieved accuracy of the overall model. Residuals of the GCPs and residuals computed on CPs are shown in Table 1. All the values confirm the centimeter-level accuracy of the 3D alignment. Moreover, a dense point cloud was generated and a classification of both ground and non-ground points was performed [46]. Finally, we generated an orthomosaic of Cell 1B (Figure 4). The georeferencing of the surveys within the same horizontal datum NAD 83 (2011) ensured a consistent comparison of the vegetated area boundaries with respect to each channel axis.

The brightening effect of clouds and the darkening effect of cloud shadows are widely known to affect remote sensing analyses, leading to inaccurate atmospheric corrections, biased estimations of spectral indices values, errors in land cover classification and false detection of land cover change. To prevent those issues that are present using multispectral UAV imageries, we captured a picture of a reflectance calibration panel immediately before, and immediately after, each flight mission, and a Downwelling Light Sensor (DLS) was also used to record lighting conditions at the time of each UAV image capture [47]. Data

processing in Agisoft Metashape took this information into account to compute a final calibrated spectral index value.

2.4. Multispectral Analysis

The two *Spartina* species were detected using the multispectral camera and computing the Normalized Difference Vegetation Index (NDVI).

Healthy plants mainly absorb light in the red bands (0.63–0.69 µm), while their cell walls strongly reflect light in the Near Infrared (NIR) band (0.7–1.1 µm), increasing the NDVI. NDVI detects changes in vegetation cover in the growing season and can be used to identify areas of vegetation stress.

In our study, we used the multispectral images retrieved during our field surveys in April 2019, May 2019, August 2019, October 2019 and November 2019. We, thus, computed NDVI and extracted the corresponding values for all the sampling points in the high and low elevation marsh area.

3. Results

3.1. Orthophoto

The high-resolution orthomosaic generated by the UAV-acquired images allowed mapping of both ecological zones represented by *S. alterniflora* and *S. pumilus* (Figure 5). The two vegetated areas were compared with the corresponding 2012 planting plan and elevations provided by the USACE. Comparisons of vegetation condition were made over about one year using the UAV surveys, and changes in vegetation distributions were compared over a seven-year time frame, from 2012 to 2019, using the UAV imagery and as-built map (Figure 5).

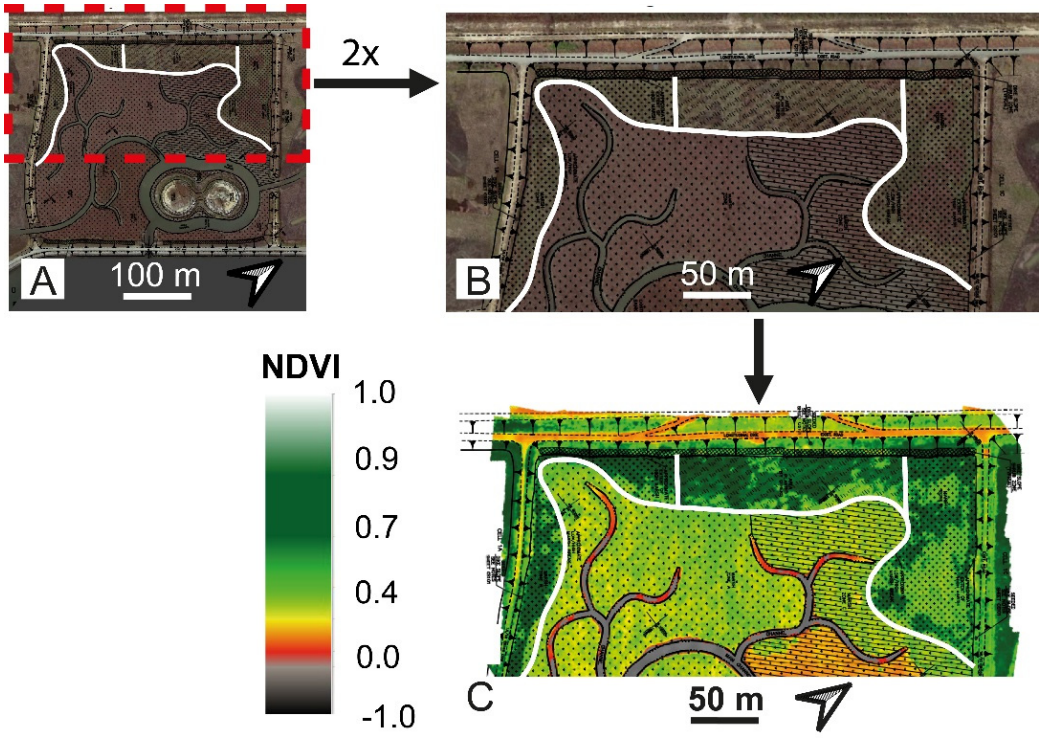

Figure 5. Maps of the initial plant configuration in Cell 1B ((**A**,**B**), and highlighted in the zoomed plot of Figure 1) a georeferenced orthophoto was combined with an NDVI map in the month of October 2019 (**C**). The white continuous line displays the original boundary between the *S. pumilus* (high marsh) and *S. alterniflora* (low marsh). Light green in plot C shows an invasion of the *S. alterniflora* into the high marsh zone of Cell 1B, reflected as a dark green.

The results of the RGB imagery processing are shown in Figure 6 for the seasonal marsh variation in Cell 1B. Spring and summer months display "greener" colors for the vegetation portion of the tidal wetland, while images from the fall season show a predominant brown color, with fewer zones still green. Figure 6 highlights visible differences between the two marsh species in response to colder temperatures.

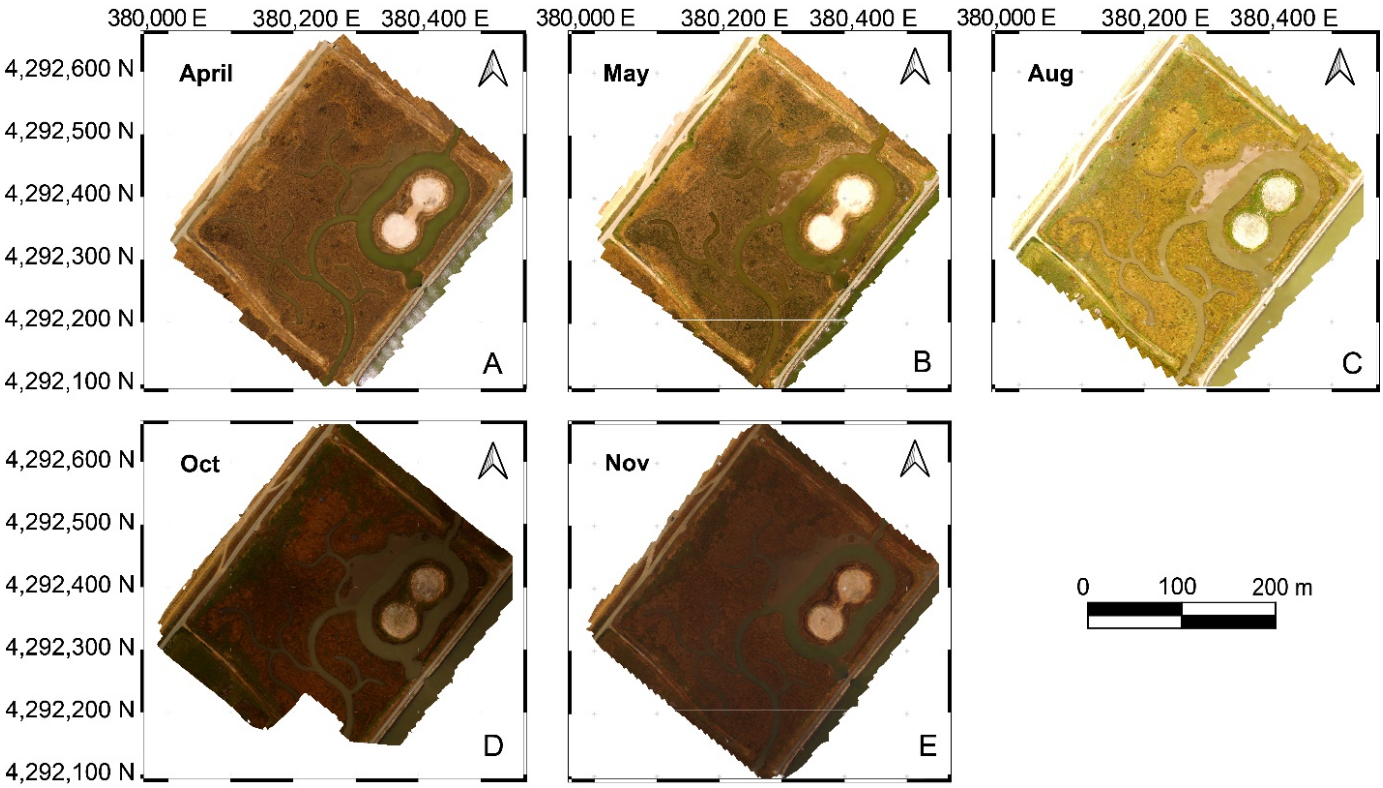

Figure 6. Orthophotos from RGB camera images elaboration for the Cell 1B in the five months surveyed. (**A**) April 2019, (**B**) May 2019, (**C**) August 2019, (**D**) October 2019 and (**E**) November 2019.

3.2. Vegetation Characterization by NDVI

The NDVI index for Cell 1B changed over the 5 considered months, reflecting vegetation growth and senescence, and it was found that the differences between the two *Spartina* species were most evident in the fall (Figure 7). April and May show the emergence of the marsh vegetation from dormancy, passing from NDVI values around 0.25 as growth begins in April, and 0.4–0.5 in May as growth continues, before reaching the peak in August, near the maximum biomass in the region and the onset of flower production [48,49], with values up to 0.7. In the fall (October and November) the different phenology of the two species becomes evident. *Spartina alterniflora* senesces earlier than *S. pumilus*. While the dead stems and leaves of *S. alterniflora* tend to decay during the winter, *S. pumilus* maintains green leaves throughout the winter [50], resulting in NDVI values in the high marsh close to 0.7 in November.

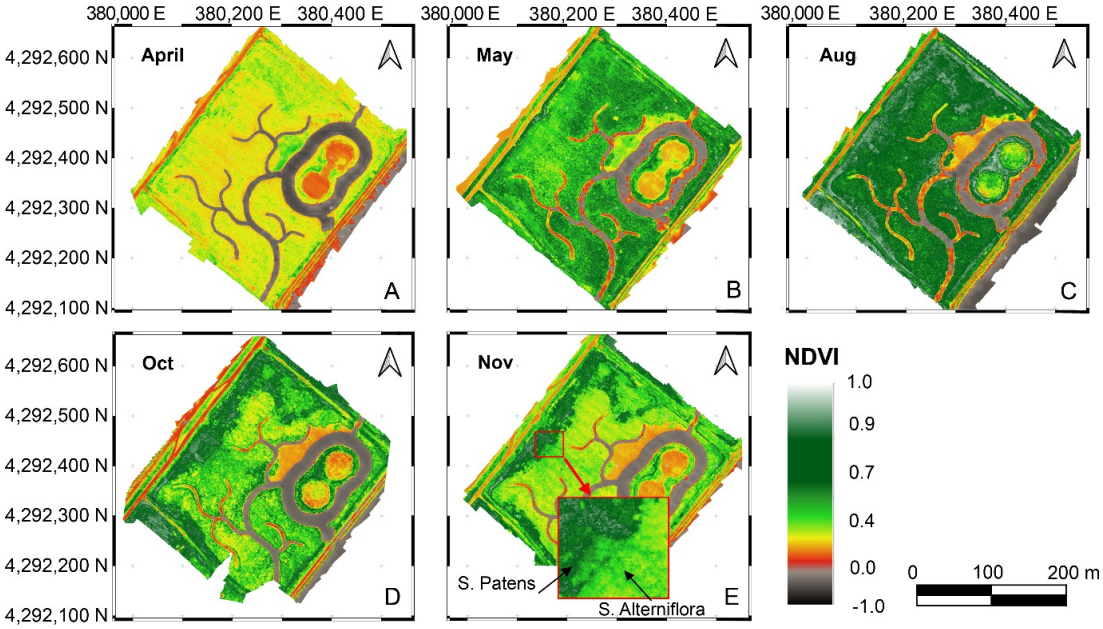

Figure 7. NDVI for Cell 1B in the five months surveyed, (**A**) April 2019, (**B**) May 2019, (**C**) August 2019, (**D**) October 2019 and (**E**) November 2019. Inset in November image shows area where *S. alterniflora* is migrating into the original high marsh zone.

3.3. Field Measurements of Marsh Characteristics

Seasonal marsh surveys showed increased vegetation volume from spring to fall (Figure 8a), a distinct difference in volume between the two species (Figure 8a,b), and a strong relationship between NDVI and vegetation volume for both species. *Spartina alterniflora* vegetation volume ranged from near 0 mm^3 in spring, prior to the emergence of new shoots, to >450,000 mm^3 in summer, as the vegetation matured, and remained high into the fall even as the plants senesced. In contrast, *S. pumilus* volume was much lower, ranging from approximately 0–85,000 mm^3.

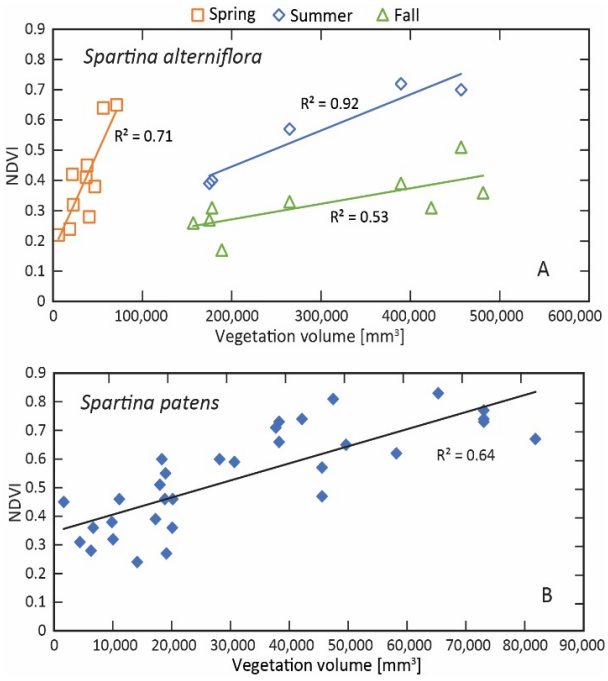

Figure 8. Vegetation characteristic from survey and remote sensing data divided by the two main marsh species present in the study site: (**A**) *Spartina alterniflora* and (**B**) *Spartina patens*. Plot (**A**) shows through colors and shapes the marsh field measurements and relative NDVI divided by the three seasons.

Spartina alterniflora NDVI followed a similar pattern from spring to summer (increasing NDVI), but decreased in the fall following senescence. There was a significant seasonal correlation between NDVI and volume for *S. alterniflora* (Spring: $R^2 = 0.71$, $p < 0.05$; Summer: $R^2 = 0.92$, $p < 0.05$; Fall: $R^2 = 0.53$, $p < 0.05$) (Figure 8a). *Sporobolus pumilus* NDVI did not show strong seasonal variation due to the persistence of green leaves throughout the year, but there was a moderately strong correlation between NDVI and vegetation volume ($R^2 = 0.64$, $p < 0.05$) (Figure 8b), with the peak NDVI occurring in the summer (Figure 9).

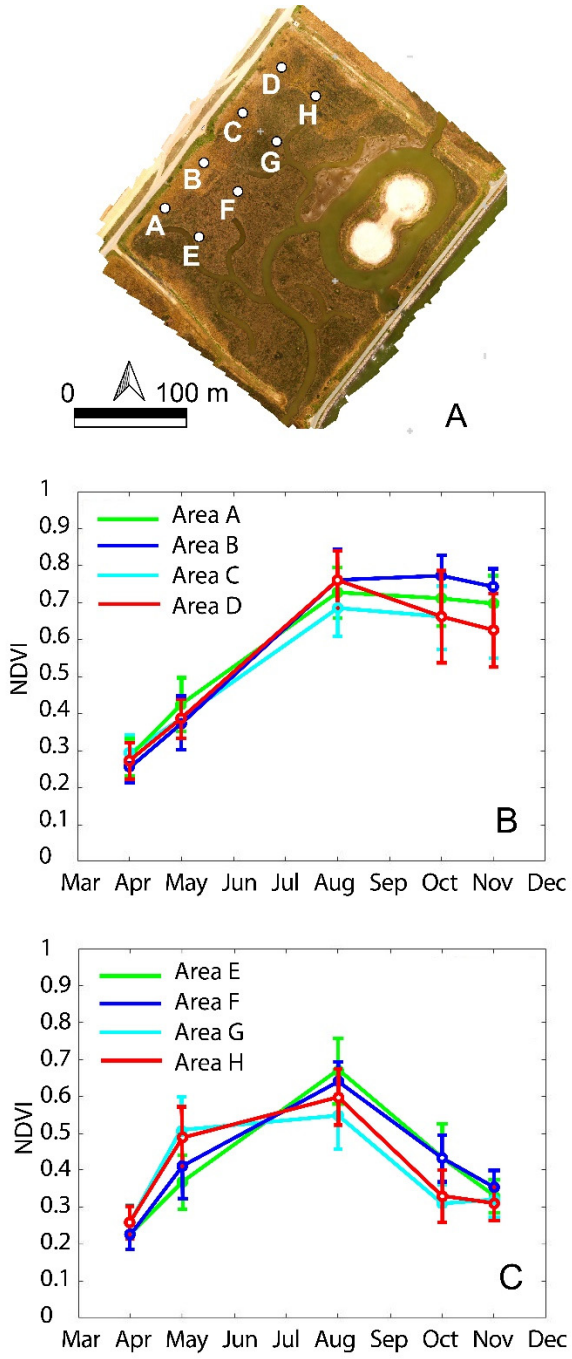

Figure 9. (**A**) Position of the 8 areas of 4 m^2. Areas A-B-C-D refer to *S. pumilus*, while E-F-G-H refer to *S. alterniflora* (orthophoto from RGB camera in May 2019). (**B**) Seasonal NDVI changes in the *S. pumilus*. (**C**) Seasonal NDVI changes in the *S. alterniflora*. The error bar refers to above and below a standard deviation.

3.4. Marsh Seasonality

Marsh seasonality has been investigated through NDVI seasonal variation of the two dominant vegetation species. We defined eight specific plots (2 m × 2 m) (Figure 9a), from which NDVI values were extracted for the 5 observed months (Table 2). The standard deviation quantifies the amount of variation with respect to the mean NDVI value in the studied plot. The reported NDVI values are the average value of each area. The results showed low NDVI values in April for both species. NDVI increased slightly more rapidly in the *S. alterniflora* plots than in the *S. pumilus* plots, but by August NDVI was higher in the *S. pumilus* plots compared with *S. alterniflora*. In the fall, NDVI decreased as *S. alterniflora* entered senescence, but remained high for *S. pumilus*, with values around 0.3–0.4 and 0.6–0.7, respectively (Figure 9).

Table 2. Monthly NDVI values in the high marsh (*S. pumilus*) and low marsh (*S. alterniflora*) zones.

April	May	August	October	November
		S. pumilus		
		Area A		
0.28	0.45	0.73	0.71	0.70
		Area B		
0.26	0.37	0.76	0.77	0.74
		Area C		
0.29	0.39	0.68	0.66	0.63
		Area D		
0.27	0.39	0.76	0.66	0.62
		S. alterniflora		
		Area E		
0.23	0.36	0.67	0.43	0.33
		Area F		
0.23	0.41	0.64	0.43	0.35
		Area G		
0.26	0.50	0.55	0.30	0.32
		Area H		
0.26	0.49	0.60	0.33	0.31

3.5. Example of Marsh Encroachment Monitoring

To detect vegetation development across the mudflat zones (Figure 10), we compared the initial vegetation extension obtained from Google Earth (October 2013), and the boundary of *S. alterniflora* on the mudflat detected by UAVs surveys between April 2019 and November 2019 (Table 3).

Table 3. UAV flights date over the Cell 1B in the five months surveyed.

Month Identification	Date (Day/Month/Year)
April 2019	3 April 2019
May 2019	2 May 2019
August 2019	29 August 2019
October 2019	3 October 2019
November 2019	14 November 2019

Figure 10 depicts the initial situation as reported from Google Earth imagery in October 2013, being the time of vegetation planting. The subsequent survey of the vegetation boundary, performed between April 2019 and November 2019, is shown in Figure 10. The colonization and migration of *S. alterniflora* toward the channel bank and the central part of the mudflat is well noticeable from the RGB orthomosaic map. The latter represents a quick method to detect the marsh evolution and colonization of *Spartina* species. The precise assessment of vegetation monitoring can be implemented through a year-by-year survey focused on the vegetation patch expansion. A seasonal analysis may be conducted to explore the most suitable period for marsh colonization or plantation.

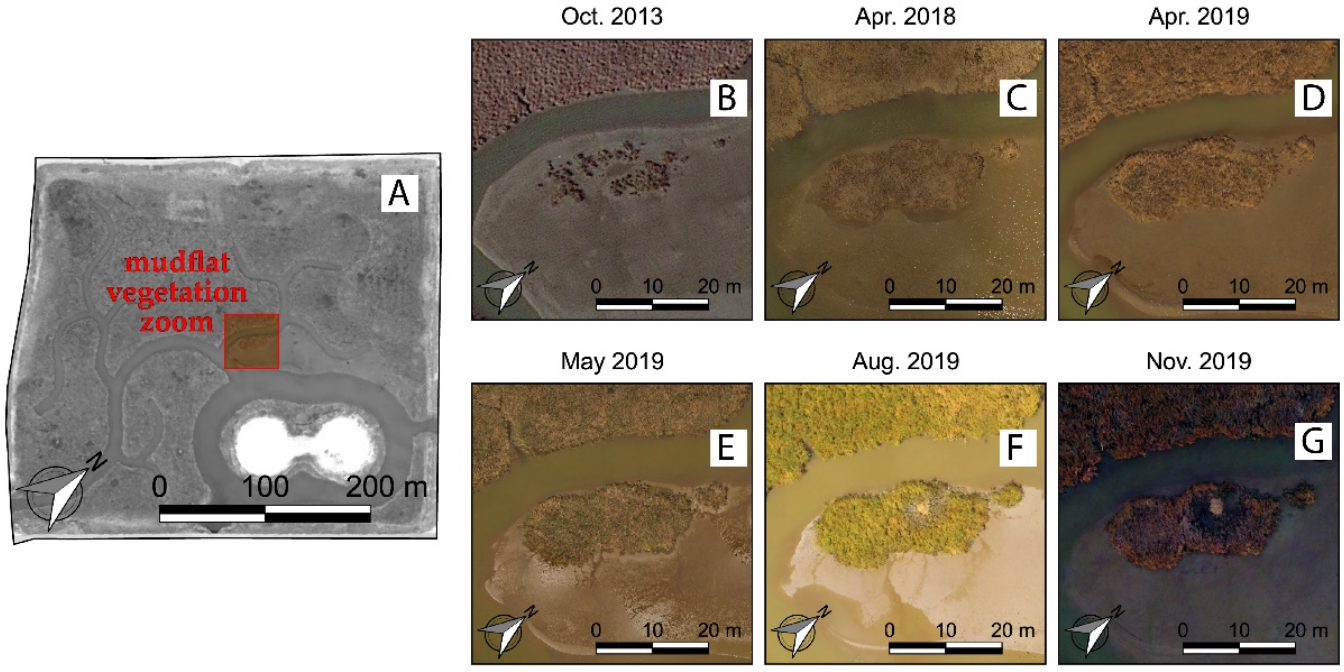

Figure 10. (**A**) Position of the mudflat. (**B**) image of the mudflat from Google Earth (October 2013). (**C**–**G**) refer to *S. alterniflora* vegetation from orthomosaic images, respectively of April 2018, April 2019, May 2019, August 2019 and November 2019. (**B**–**G**) represents a zoom of the red square in plot **A**.

4. Discussion

4.1. Coastal Wetlands Monitoring by UAVs

The results of this study demonstrate that vegetation mapping, obtained from high-resolution multispectral UAV observations for a 400 by 400-m wetland, are in good agreement with direct observations and field measurements. Indeed, UAVs combined with field measurements, provide very high-resolution vegetation maps of vegetation in restored and engineered marshes, allowing for the identification of wetland vegetation dynamics, almost in real-time. Seasonality and vegetation species migration are recognizable from the maps produced from MSI analysis using high resolution UAV imagery, thereby introducing this new methodology for monitoring spatial and temporal changes at high resolution for coastal wetland management. Based on the ability to conduct UAV surveys frequently and on short notice, UAV monitoring may be implemented ahead of extreme events, such as severe storms or hurricanes to monitor and quantify their impacts on coastal wetlands.

4.2. Vegetation Species Characterization

Our study showed how high-resolution data can help to identify and to estimate the vegetation density of the two dominant marsh vegetation species, *S. alterniflora* and *S. pumilus*. Such results have also been obtained by Doughty and Cavanaugh (2019) [31] who mapped the biomass in coastal wetlands using high-resolution multispectral UAV imagery.

In the present study, the high-resolution multispectral images have allowed us to monitor the annual growth and development of two species: *S. alterniflora* and *S. pumilus*.

Additionally, this study demonstrates that the NDVI values from the multispectral camera can be applied to assess and monitor the growth stage of vegetation, as already observed by other studies [25,51,52]. Indeed, the results show a good correlation between the NDVI (a commonly used proxy for vegetation health and productivity) and the measured vegetation characteristics in the field (allowing us to assess the growth stage of the vegetation). Before new growth begins in early spring, standing dead vegetation has lower levels of chlorophyll, which absorbs light in the blue and red wavelengths and has a reflectance peak in the green. The result is lower NDVI in late fall through early spring, and peak NDVI in summer when the vegetation matures. The results were also confirmed by the RGB aero-photos showing that marshes, still in the dormancy phase, with an "autumn-winter" coloration. A "red" coloration was observed due to the absence of chlorophyll. Similar results were observed by Doughty and Cavanaugh (2019) [30] who found that in the California coastal marshes, a pronounced seasonal variability was observed in vegetation health and biomass, characterized by a green-up of vegetation in spring with a biomass peak at the end of summer.

Importantly, our study shows that NDVI also reveals the different growth patterns for the two marsh species. In particular, *S. alterniflora* has slightly faster spring growth compared to *S. pumilus*, but senesces in fall before entering dormancy in the mid-Atlantic region. During the summer (in August), *S. pumilus* has a higher NDVI. This may be due to higher tissue chlorophyll *a* concentration, allowing the absorption of more ultraviolet, blue and red rays and reflection of more green and infrared rays, compared to *S. alterniflora*. It may also reflect the differing morphology of the two species. *Spartina alterniflora* has stiff stems and leaves oriented vertically, while *S. pumilus* has thin stems and leaves that are often decumbent.

During the autumn, the NDVI index captures the decay of *S. alterniflora* aboveground biomass and the persistent green shoots of *S. pumilus*, in agreement with the species growth pattern, and again related to the marsh stem morphology and structure [53,54]. The differences in morphology and growth patterns between these two dominant marsh species allows for the potential to differentiate between them in high resolution imagery using MSI analysis. This study indicates that the optimal time of year for mapping aerial coverage of each species, and distinguishing between high marsh and low marsh, is after *S. alterniflora* senescence in the fall, followed by winter until new growth begins in the spring. Summer is the least advantageous time to acquire imagery to differentiate the two species.

Through an examination of time series high resolution imagery and MSI analysis, it may be possible to estimate rates of marsh transgression. While rates of erosion at the marsh edge and marsh transgression into the uplands have been estimated from aerial imagery [55], the more subtle migration of low marsh vegetation into the high marsh has been more difficult to detect. The methodology presented here may be used to identify these areas of internal marsh transgression, where *S. alterniflora* is migrating from the low marsh into areas that were formerly high marsh occupied by *S. pumilus*, a process driven by especially high rates of sea level rise in the mid-Atlantic region [56].

The differences in vegetation characteristics during the fall season depend on different factors such as: the action of waves, the turbidity, the deposition of fine sediment and the sea level, which is generally higher during the fall. The higher frequency of flooding is also related to increased phenomena of nuisance flooding and sea level rise registered in the Chesapeake Bay. In fact, the Chesapeake Bay is the Nation's largest estuary, and its natural resources are intimately connected to the history, culture, and local economies of the counties and towns lining its shores. Sea Level Rise (SLR) is especially rapid in Chesapeake Bay; impacts of rising sea levels are pronounced along its Eastern Shore of Maryland, due to low elevations and gentle gradients.

Parts of the Eastern Shore lie within the boundaries of the Miles River and Choptank River and represent some of Maryland's most climate vulnerable coasts. Local SLR predic-

tions are 2.1 feet and 5.7 feet by 2050 and 2100 [57,58], respectively, which will result in a loss of tens of thousands of acres of wetlands habitat. Consequently, there is a growing call for Natural Nature-Based Features (NNBF: marshes, oyster reefs, mangroves) to be not only the basis of shoreline armoring projects in the future but also to modify and improve the performance of existing shoreline infrastructure [59,60].

Another important application of RGB and multispectral imagery is the opportunity of identifying the marsh scarp or marsh boundaries since salt marsh vegetation usually ends at a drop in elevation which might be a channel or a shoreline edge as indicated by Farris et al. (2019) [61]. Indeed, as reported by Klemas (2015) [62], digital surface models (DSMs) and the digital mapping of topography provide powerful databases used to understand, model, and analyze terrestrial environments and landscapes.

The results of this study have also demonstrated the importance of the UAV images for enhancing our knowledge and understanding of saltmarsh processes and vegetation development. Indeed, the study has demonstrated the advantages and flexibility of UAV imagery to obtain multi-temporal and multispectral images useful for monitoring inaccessible areas of saltmarsh compared to traditional approaches and to develop temporal datasets that may be useful for modeling purposes. Such advantages are similar to those obtained from other remotely sensed elevation imagery such as LIDAR data [4,63]. In addition, the use of UAV techniques is less time-consuming compared to traditional survey, which represents an advantage for such inaccessible environments.

4.3. Methodological Limitations and Future Advances

A key limitation for UAV use is the limited spatial scale that can be covered, due to battery limitations, compared with satellite imagery. While satellite imagery can cover several square kilometers with a pixel size that varies from 0.5 to 10 m resolution [64], UAV surveys can cover hectares to a few square kilometers, but with a pixel resolution of a few centimeters.

In our study, marshes are characterized as vegetation volume, which allows modelers to include marsh characteristics in numerical models. However, a more useful characterization for ecological studies and restoration monitoring might include indicators of the eco-physiological processes to assess vegetation health, as well as the overall health of salt-marsh communities facing eutrophication, sea level rise and seaward erosion [65]. Additionally, single plant characteristics such as leaf area and orientation may significantly impact NDVI values. Future combined field and remote sensing studies will address these ecological components to enhance marsh characterization.

The methodology needs multiple improvements to enhance vegetation characterization and classification, including: (1) Accounting for environmental conditions, such as water level and soil moisture, which are dominant issues in tidal systems that may affect the reflectance in the near-infrared and consequently affect the assessment of the vegetation state (NDVI); and (2) automatic classification or semi-automatic classification, calibration of the UAV images, which will be essential to avoid misclassification and reduce lens distortion, as indicated by Myers et al. (2018) [66]. Therefore, further research is needed to define algorithms and rules for the UAVs images classification. However, coastal management, ecological monitoring and marsh restoration strategies depend on the developments of new technologies and methodologies for high-resolution temporal and spatial scale.

5. Conclusions

This work highlights how an integrated approach combining vegetation characterization surveying and the acquisition of aerial imageries by UAV can be successfully applied in the field of coastal monitoring and restoration interventions. The very high spatial resolution of the final orthomosaic and NDVI maps, especially if further combined with a high temporal resolution in terms of small-time lapse between survey repetitions, can lead to efficient and reliable results. Moreover, the vegetation characteristics data are practically

continuous due to the very small pixel size of the final NDVI products, if compared to a traditional and time-consuming vegetation survey.

Further survey repetitions by UAV in the future will provide more data to accurately assess the behavior of the Cell 1B system and allow managers better tools to assess ecological characterization in marsh restoration projects. Accessibility of inexpensive UAVs will allow us to increase the temporal and spatial resolution of aerial photogrammetry and datasets. High frequency data will allow scientists to quantify significant coastal processes affecting wetlands, which are presently analyzed primarily through field-based monitoring. Numerical models of wetland morphodynamics must integrate these new high resolution remote sensing products.

Author Contributions: Conceptualization W.N., Y.T., M.Q. and A.P.; methodology, W.N., Y.T., M.Q. and A.P.; software, W.N., Y.T., M.Q., G.F. and A.P.; validation, W.N., I.V., C.C., M.Q. and L.W.S.; formal analysis, W.N., Y.T., M.Q. and A.P.; investigation, W.N., Y.T., M.Q. and A.P.; resources, W.N., G.F., L.W.S. and A.P.; data curation, W.N., I.V., C.C., M.Q., G.F. and L.W.S.; writing—original draft preparation, Y.T. and W.N.; writing—review and editing, W.N., Y.T., M.Q., I.V., G.F., A.P. and L.W.S.; visualization, W.N., Y.T. and M.Q.; supervision, W.N.; project administration, W.N. and L.W.S.; funding acquisition, W.N., G.F., L.W.S. and A.P. All authors have read and agreed to the published version of the manuscript.

Funding: This research was funded by (i) University of Maryland; and (ii) Salisbury University (Faculty Mini–Grant entitled Image Acquisition by Drone to Model Coastal Areas in Chesapeake Bay).

Institutional Review Board Statement: Not Applicable.

Informed Consent Statement: Not Applicable.

Data Availability Statement: Not Applicable.

Acknowledgments: The authors are grateful to the University of Maryland Center for Environmental Science—Horn Point Laboratory, to the Maryland Environmental Service, Maryland Department of Transportation Maryland Port Administration and to the U.S. Army Corps of Engineers—Baltimore District for making possible and funding this applied research project. Partial financial support for this research was provided by the Maryland Department of Transportation Maryland Port Administration with project management by the Maryland Environmental Service. Reviews by Michelle Osborn and Claire Ruark improved this manuscript. We thank Mahdi Khademishamami, Mattia Mazzarino, Cecilia Magri, Weilun Gao, Court Stevenson, Jeff Cornwell, Mike Owens and Ashley Hollins for the assistance during field surveys. We thank Journal Editors and three anonymous reviewers for suggestions and comments which enhanced the scientific quality of the manuscript. This is contribution number 6060 of the University of Maryland Center for Environmental Science—Horn Point Laboratory.

Conflicts of Interest: The authors declare no conflict of interest.

References

1. Moffett, K.B.; Nardin, W.; Silvestri, S.; Wang, C.; Temmerman, S. Multiple Stable States and Catastrophic Shifts in Coastal Wetlands: Progress, Challenges, and Opportunities in Validating Theory Using Remote Sensing and Other Methods. *Remote Sens.* **2015**, *7*, 10184–10226. [CrossRef]
2. Nardin, W.; Larsen, L.; Fagherazzi, S.; Wiberg, P. Tradeoffs among hydrodynamics, sediment fluxes and vegetation community in the Virginia Coast Reserve, USA. *Estuar. Coast. Shelf Sci.* **2018**, *210*, 98–108. [CrossRef]
3. Fleri, J.R.; Lera, S.; Gerevini, A.; Staver, L.; Nardin, W. Empirical observations and numerical modelling of tides, channel morphology, and vegetative effects on accretion in a restored tidal marsh. *Earth Surf. Process. Landf.* **2019**, *44*, 2223–2235. [CrossRef]
4. Fagherazzi, S.; Mariotti, G.; Leonardi, N.; Canestrelli, A.; Nardin, W.; Kearney, W.S. Salt Marsh Dynamics in a Period of Accelerated Sea Level Rise. *J. Geophys. Res. Earth Surf.* **2020**, *125*. [CrossRef]
5. Barbier, E.B.; Hacker, S.D.; Kennedy, C.; Koch, E.W.; Stier, A.; Silliman, B. The value of estuarine and coastal ecosystem services. *Ecol. Monogr.* **2011**, *81*, 169–193. [CrossRef]
6. Fourqurean, J.; Duarte, C.M.; Kennedy, H.; Marbà, N.; Holmer, M.; Mateo, M.; Apostolaki, E.; Kendrick, G.; Krause-Jensen, D.; McGlathery, K.J.; et al. Seagrass ecosystems as a globally significant carbon stock. *Nat. Geosci.* **2012**, *5*, 505–509. [CrossRef]
7. Sallenger, A.H.; Doran, K.; Howd, P.A. Hotspot of accelerated sea-level rise on the Atlantic coast of North America. *Nat. Clim. Chang.* **2012**, *2*, 884–888. [CrossRef]

8. Cronin, W.B. *The Disappearing Islands of the Chesapeake*; Johns Hopkins University Press: Baltimore, MD, USA, 2005.
9. Craft, C.; Clough, J.; Ehman, J.; Joye, S.; Park, R.; Pennings, S.; Guo, H.; Machmuller, M. Forecasting the effects of accelerated sea-level rise on tidal marsh ecosystem services. *Front. Ecol. Environ.* **2009**, *7*, 73–78. [CrossRef]
10. Russ, E.R.; Palinkas, C. Seasonal-Scale and Decadal-Scale Sediment-Vegetation Interactions on the Subaqueous Susquehanna River Delta, Upper Chesapeake Bay. *Chesap. Sci.* **2018**, *41*, 2092–2104. [CrossRef]
11. Mudd, S.M.; Fagherazzi, S.; Morris, J.T.; Furbish, D.J. Flow, sedimentation, and biomass production on a vegetated salt marsh in South Carolina: Toward a predictive model of marsh morphologic and ecologic evolution. *Ecogeomorphol. Tidal Marshes Coast. Estuar. Stud.* **2004**, *59*, 165–187.
12. Morris, J.T.; Sundareshwar, P.V.; Nietch, C.T.; Kjerfve, B.; Cahoon, D.R. Responses of coastal wetlands to rising sea level. *Ecology* **2002**, *83*, 2869–2877. [CrossRef]
13. Temmerman, S.; Bouma, T.J.; Govers, G.; Wang, Z.B.; De Vries, M.; Herman, P. Impact of vegetation on flow routing and sedimentation patterns: Three-dimensional modeling for a tidal marsh. *J. Geophys. Res. Space Phys.* **2005**, *110*. [CrossRef]
14. Kirwan, M.L.; Murray, A.B. A coupled geomorphic and ecological model of tidal marsh evolution. *Proc. Natl. Acad. Sci. USA* **2007**, *104*, 6118–6122. [CrossRef] [PubMed]
15. Fagherazzi, S.; Kirwan, M.L.; Mudd, S.M.; Guntenspergen, G.R.; Temmerman, S.; D'Alpaos, A.; Van De Koppel, J.; Rybczyk, J.M.; Reyes, E.; Craft, C.B.; et al. Numerical models of salt marsh evolution: Ecological, geomorphic, and climatic factors. *Rev. Geophys.* **2012**, *50*. [CrossRef]
16. Leonard, L.A.; Croft, A.L. The effect of standing biomass on flow velocity and turbulence in Spartina alterniflora canopies. *Estuar. Coast. Shelf Sci.* **2006**, *69*, 325–336. [CrossRef]
17. Anderson, M.; Smith, J. Wave attenuation by flexible, idealized salt marsh vegetation. *Coast. Eng.* **2013**, *83*, 82–92. [CrossRef]
18. Ward, L.G.; Kemp, W.M.; Boynton, W. The influence of waves and seagrass communities on suspended particulates in an estuarine embayment. *Mar. Geol.* **1984**, *59*, 85–103. [CrossRef]
19. Kumar, L.; Sinha, P. Mapping salt-marsh land-cover vegetation using high-spatial and hyperspectral satellite data to assist wetland inventory. *GISci. Remote Sens.* **2014**, *51*, 483–497. [CrossRef]
20. Sun, C.; Fagherazzi, S.; Liu, Y. Classification mapping of salt marsh vegetation by flexible monthly NDVI time-series using Landsat imagery. *Estuar. Coast. Shelf Sci.* **2018**, *213*, 61–80. [CrossRef]
21. Nardin, W.; Vona, I.; Fagherazzi, S. Sediment deposition affects mangrove forests in the Mekong delta, Vietnam. *Cont. Shelf Res.* **2020**, *213*, 104319. [CrossRef]
22. Taddia, Y.; Nardin, W.; Corbau, C.; Franchi, G.; Stevenson, C.J.; Staver, L.W. Channels' shape evolution detected by UAVs in a restored salt marsh. In *Coastal Sediments*; World Scientific: Singapore, 2019; pp. 1519–1527.
23. Adão, T.; Hruška, J.; Pádua, L.; Bessa, J.; Peres, E.; Morais, R.; Sousa, J.J. Hyperspectral Imaging: A Review on UAV-Based Sensors, Data Processing and Applications for Agriculture and Forestry. *Remote Sens.* **2017**, *9*, 1110. [CrossRef]
24. Staver, L.W.; Stevenson, J.C.; Cornwell, J.C.; Nidzieko, N.J.; Owens, M.S.; Logan, L.; Kim, C.; Malkin, S.Y. Tidal Marsh Restoration at Poplar Island: II. Elevation Trends, Vegetation Development, and Carbon Dynamics. *Wetlands* **2020**, *40*, 1687–1701. [CrossRef]
25. Nardin, W.; Edmonds, D.; Fagherazzi, S. Influence of vegetation on spatial patterns of sediment deposition in deltaic islands during flood. *Adv. Water Resour.* **2016**, *93*, 236–248. [CrossRef]
26. Bullock, E.L.; Fagherazzi, S.; Nardin, W.; Vo-Luong, P.; Nguyen, P.; Woodcock, C.E. Temporal patterns in species zonation in a mangrove forest in the Mekong Delta, Vietnam, using a time series of Landsat imagery. *Cont. Shelf Res.* **2017**, *147*, 144–154. [CrossRef]
27. Díaz-Delgado, R.; Cazacu, C.; Adamescu, M. Rapid Assessment of Ecological Integrity for LTER Wetland Sites by Using UAV Multispectral Mapping. *Drones* **2018**, *3*, 3. [CrossRef]
28. Martin, F.-M.; Müllerová, J.; Borgniet, L.; Dommanget, F.; Breton, V.; Evette, A. Using Single- and Multi-Date UAV and Satellite Imagery to Accurately Monitor Invasive Knotweed Species. *Remote Sens.* **2018**, *10*, 1662. [CrossRef]
29. Villoslada, M.; Bergamo, T.; Ward, R.; Burnside, N.; Joyce, C.; Bunce, R.; Sepp, K. Fine scale plant community assessment in coastal meadows using UAV based multispectral data. *Ecol. Indic.* **2020**, *111*, 105979. [CrossRef]
30. Doughty, C.L.; Cavanaugh, K.C. Mapping Coastal Wetland Biomass from High Resolution Unmanned Aerial Vehicle (UAV) Imagery. *Remote Sens.* **2019**, *11*, 540. [CrossRef]
31. Ali, I.; Cawkwell, F.; Dwyer, E.; Barrett, B.; Green, S. Satellite remote sensing of grasslands: From observation to management. *J. Plant Ecol.* **2016**, *9*, 649–671. [CrossRef]
32. Baena, S.; Moat, J.; Whaley, O.; Boyd, D. Identifying species from the air: UAVs and the very high resolution challenge for plant conservation. *PLoS ONE* **2017**, *12*, e0188714. [CrossRef]
33. Cornwell, J.C.; Owens, M.S.; Staver, L.W.; Stevenson, J.C. Tidal Marsh Restoration at Poplar Island I: Transformation of Estuarine Sediments into Marsh Soils. *Wetlands* **2020**, *40*, 1673–1686. [CrossRef]
34. Kelly, W.; Paul, S. Sarbanes Ecosystem Restoration Project at Poplar Island. In *Engineering for Sustainable Communities: Principles and Practices*; US Army Corps of Engineering: Baltimore, MD, USA, 2017; pp. 411–417.
35. Kent, J. *Water Level Variations at Poplar Island, MD*; NOAA Technical Report NOS-OPS 076; NOAA: Silver Spring, MD, USA, 2015.
36. Drummond, C.D.; Harley, M.D.; Turner, I.L.; A Matheen, A.N.; Glamore, W.C. UAV applications to coastal engineering. In Proceedings of the Australasian Coasts & Ports Conference 2015: 22nd Australasian Coastal and Ocean Engineering Conference and the 15th Australasian Port and Harbour Conference, Auckland, New Zealand, 15–18 September 2015; p. 267.

37. Clapuyt, F.; Vanacker, V.; Van Oost, K. Reproducibility of UAV-based earth topography reconstructions based on Structure-from-Motion algorithms. *Geomorphology* **2016**, *260*, 4–15. [CrossRef]
38. Turner, I.L.; Harley, M.; Drummond, C.D. UAVs for coastal surveying. *Coast. Eng.* **2016**, *114*, 19–24. [CrossRef]
39. Watanabe, Y.; Kawahara, Y. UAV Photogrammetry for Monitoring Changes in River Topography and Vegetation. *Procedia Eng.* **2016**, *154*, 317–325. [CrossRef]
40. Mancini, F.; Dubbini, M.; Gattelli, M.; Stecchi, F.; Fabbri, S.; Gabbianelli, G. Using Unmanned Aerial Vehicles (UAV) for High-Resolution Reconstruction of Topography: The Structure from Motion Approach on Coastal Environments. *Remote Sens.* **2013**, *5*, 6880–6898. [CrossRef]
41. Hugenholtz, C.H.; Whitehead, K.; Brown, O.W.; Barchyn, T.E.; Moorman, B.; LeClair, A.; Riddell, K.; Hamilton, T. Geomorphological mapping with a small unmanned aircraft system (sUAS): Feature detection and accuracy assessment of a photogrammetrically-derived digital terrain model. *Geomorphology* **2013**, *194*, 16–24. [CrossRef]
42. Casella, E.; Rovere, A.; Pedroncini, A.; Stark, C.P.; Casella, M.; Ferrari, M.; Firpo, M. Drones as tools for monitoring beach topography changes in the Ligurian Sea (NW Mediterranean). *Geo-Mar. Lett.* **2016**, *36*, 151–163. [CrossRef]
43. James, M.; Robson, S.; D'Oleire-Oltmanns, S.; Niethammer, U. Optimising UAV topographic surveys processed with structure-from-motion: Ground control quality, quantity and bundle adjustment. *Geomorphology* **2017**, *280*, 51–66. [CrossRef]
44. Westoby, M.J.; Brasington, J.; Glasser, N.F.; Hambrey, M.J.; Reynolds, J.M. 'Structure-from-Motion'photogrammetry: A low-cost, effective tool for geoscience applications. *Geomorphology* **2012**, *179*, 300–314. [CrossRef]
45. Cook, K. An evaluation of the effectiveness of low-cost UAVs and structure from motion for geomorphic change detection. *Geomorphology* **2017**, *278*, 195–208. [CrossRef]
46. Agisoft, L.L.C. PhotoScan User Manual, Professional Edition, Version 1.4. 2018. Available online: http://www.agisoft.com/pdf/photoscan-pro_1_4_en.pdf (accessed on 1 October 2018).
47. Taddia, Y.; Russo, P.; Lovo, S.; Pellegrinelli, A. Multispectral UAV monitoring of submerged seaweed in shallow water. *Appl. Geomat.* **2019**, *12*, 19–34. [CrossRef]
48. Pomeroy, L.R.; Darley, W.M.; Dunn, E.L.; Gallagher, J.L.; Haines, E.B.; Whitney, D.M. Primary Production. In *The Ecology of a Salt Marsh*; Springer: Berlin/Heidelberg, Germany, 1981; pp. 39–67.
49. Gallagher, J.L.; Somers, G.F.; Grant, D.M.; Seliskar, D.M. Persistent Differences in Two Forms of Spartina Alterniflora: A Common Garden Experiment. *Ecology* **1988**, *69*, 1005–1008. [CrossRef]
50. Lonard, R.I.; Judd, F.W.; Stalter, R. The Biological Flora of Coastal Dunes and Wetlands: Spartina patens (W. Aiton) G.H. Muhlenberg. *J. Coast. Res.* **2010**, *265*, 935–946. [CrossRef]
51. Al-Ali, Z.M.; Abdullah, M.; Asadalla, N.B.; Gholoum, M. A comparative study of remote sensing classification methods for monitoring and assessing desert vegetation using a UAV-based multispectral sensor. *Environ. Monit. Assess.* **2020**, *192*, 389. [CrossRef]
52. Wahab, I.; Hall, O.; Jirström, M. Remote Sensing of Yields: Application of UAV Imagery-Derived NDVI for Estimating Maize Vigor and Yields in Complex Farming Systems in Sub-Saharan Africa. *Drones* **2018**, *2*, 28. [CrossRef]
53. Hill, T.D.; Roberts, B.J. Effects of seasonality and environmental gradients on Spartina alterniflora allometry and primary production. *Ecol. Evol.* **2017**, *7*, 9676–9688. [CrossRef] [PubMed]
54. Raposa, K.B.; Wasson, K.; Smith, E.; Crooks, J.A.; Delgado, P.; Fernald, S.H.; Ferner, M.C.; Helms, A.; Hice, L.A.; Mora, J.W.; et al. Assessing tidal marsh resilience to sea-level rise at broad geographic scales with multi-metric indices. *Biol. Conserv.* **2016**, *204*, 263–275. [CrossRef]
55. Schieder, N.W.; Walters, D.C.; Kirwan, M.L. Massive Upland to Wetland Conversion Compensated for Historical Marsh Loss in Chesapeake Bay, USA. *Chesap. Sci.* **2017**, *41*, 940–951. [CrossRef]
56. Alizad, K.; Hagen, S.C.; Medeiros, S.C.; Bilskie, M.V.; Morris, J.T.; Balthis, L.; Buckel, C.A. Dynamic responses and implications to coastal wetlands and the surrounding regions under sea level rise. *PLoS ONE* **2016**, *13*, e0205176. [CrossRef] [PubMed]
57. Boesch, D.F.; Atkinson, L.P.; Boicourt, W.C.; Boon, J.D.; Cahoon, D.R.; Dalrymple, R.; Ezer, T.A.; Horton, B.P.; Johnson, Z.P.; Kopp, R.E.; et al. *Updating Maryland's Sea-Level Rise Projections*; Special Report of the Scientific and Technical Working Group to the Maryland Climate Change Commission; University of Maryland Center for Environmental Science: Cambridge, MD, USA, 2013; 22p.
58. Boesch, D.F.; Boicourt, W.C.; Cullather, R.I.; Ezer, T.; Galloway, G.E., Jr.; Johnson, Z.P.; Kilbourne, K.H.; Kirwan, M.L.; Kopp, R.E.; Land, S.; et al. *Sea-Level Rise: Projections for Maryland*; University of Maryland Center for Environmental Science: Cambridge, MD, USA, 2018; 27p.
59. Sutton-Grier, A.E.; Wowk, K.; Bamford, H. Future of our coasts: The potential for natural and hybrid infrastructure to enhance the resilience of our coastal communities, economies and ecosystems. *Environ. Sci. Policy* **2015**, *51*, 137–148. [CrossRef]
60. Sutton-Grier, A.; Gittman, R.; Arkema, K.; Bennett, R.; Benoit, J.; Blitch, S.; Burks-Copes, K.; Colden, A.; Dausman, A.; DeAngelis, B.; et al. Investing in Natural and Nature-Based Infrastructure: Building Better Along Our Coasts. *Sustainability* **2018**, *10*, 523. [CrossRef]
61. Farris, A.S.; Defne, Z.; Ganju, N.K. Identifying Salt Marsh Shorelines from Remotely Sensed Elevation Data and Imagery. *Remote Sens.* **2019**, *11*, 1795. [CrossRef]
62. Klemas, V.V. Coastal and Environmental Remote Sensing from Unmanned Aerial Vehicles: An Overview. *J. Coast. Res.* **2015**, *315*, 1260–1267. [CrossRef]

63. Pinton, D.; Canestrelli, A.; Fantuzzi, L. A UAV-Based Dye-Tracking Technique to Measure Surface Velocities over Tidal Channels and Salt Marshes. *J. Mar. Sci. Eng.* **2020**, *8*, 364. [CrossRef]
64. Toth, C.; Jóźków, G. Remote sensing platforms and sensors: A survey. *ISPRS J. Photogramm. Remote Sens.* **2016**, *115*, 22–36. [CrossRef]
65. Collin, A.; Long, B.; Archambault, P. Salt-marsh characterization, zonation assessment and mapping through a dual-wavelength LiDAR. *Remote Sens. Environ.* **2010**, *114*, 520–530. [CrossRef]
66. Myers, D.J.; Schweik, C.M.; Wicks, R.; Bowlick, F.; Carullo, M. Developing a land cover classification of salt marshes using uas time-series imagery and an open source workflow. *ISPRS Int. Arch. Photogramm. Remote Sens. Spat. Inf. Sci.* **2018**, *42*, 155–162. [CrossRef]